THE AMERICAN SOCIETY OF MECHANICAL ENGINEERS
345 E. 47th St., New York, N.Y. 10017

93-GT-52

TURBULENCE MEASUREMENTS DOWNSTREAM OF A TURBINE CASCADE AT DIFFERENT INCIDENCE ANGLES AND PITCH-CHORD RATIOS

Vincenzo Dossena
Dipartimento di Energetica
Politecnico di Milano
Milan, Italy

Antonio Perdichizzi
Dipartimento di Meccanica
Università di Bergamo
Brescia, Italy

Marina Ubaldi and Pietro Zunino
Dipartimento di Ingegneria Energetica
Università di Genova
Genoa, Italy

ABSTRACT

An experimental investigation on a linear turbine cascade has been carried out to study the effects induced by incidence angle and pitch-chord ratio variations on the three-dimensional turbulent flow downstream of the cascade.

Previous mean flow measurements have shown how these parameters influence the energy losses and the secondary velocity field. Now detailed hot wire measurements have been performed on a plane located at 22 per cent of an axial chord downstream of the trailing edge, in order to determine the distribution of all the six Reynolds stress tensor components, for three incidence conditions (i = -30, 0, +30 deg) and for three pitch-chord ratios (s/c = 0.58, 0.72, 0.87).

Significant changes of the turbulent flow structure, interesting magnitude and distribution of the Reynolds stress components, have been observed for all the considered test conditions.

The analysis of the results shows the correlation between the mean flow features and the turbulent quantities and the relationship between the energy loss production and the blade loading variation.

The presented data are also suitable for assessing the behaviour of turbulence models in complex 3D flows, on design and off-design conditions.

NOMENCLATURE

b	blade axial chord
c	blade chord
h	blade height
i	incidence angle
M	Mach number
P	turbulence production term $P = -\Sigma_{ij}\,\overline{u_i u_j}\,U_{i,j}$
q	turbulence kinetic energy coefficient $q = (\overline{u^2} + \overline{v^2} + \overline{w^2})/U_1^2$
Re_2	outlet isentropic Reynolds number based on the chord $Re_2 = U_{2is}c/\nu_1$
s	pitch
SKE	secondary kinetic energy coefficient $SKE = (V_2^2 + W_2^2)/U_{2is}$
S_{ij}	mean strain tensor $S_{ij} = U_{i,j} + U_{j,i}$
s, n, z	flow coordinate system, s direction of the undisturbed flow at midspan, n normal, z spanwise direction
Tu	turbulence intensity $Tu = (q/3)^{1/2}$
U, u	mean and fluctuating streamwise velocity components
U_i, u_i	mean and fluctuating velocity components
U_1	upstream freestream velocity
U_{2is}	downstream isentropic velocity
U^*	local mean velocity $U^* = (U^2 + V^2 + W^2)^{1/2}$
V, v	mean and fluctuating transverse velocity components
W, w	mean and fluctuating spanwise velocity components
x, y, z	cascade coordinate system (Fig. 1)
x_i	flow coordinates
β	flow angle (from tangential direction)
β'	blade angle (from tangential direction)
ζ	energy loss coefficient $\zeta = [U_{2is}^{*2}(y,z) - U_2^{*2}(y,z)] \,/\, U_{2is,MS}^2$
ν_1	laminar kinematic viscosity
ν_{ij}	eddy kinematic viscosities

Subscripts

is	isentropic condition
MS	midspan
1	upstream of the cascade
2	downstream of the cascade

Overbars

—	time averaged

1. INTRODUCTION

The continuous request of additional improvements in gas turbine design presses to achieve a deeper knowledge of the complex fluid-dynamic phenomena occurring in high pressure turbine stages. As well known, due to the low aspect ratios of such bladings, the secondary flow effects become generally relevant and are often responsible for a significant amount of the total losses. In order to get an optimum design, detailed information about the influence of various design parameters is needed and extensive aerodynamic analyses of the 3D flow have to be performed both for design and off-design conditions.

In the last years the aerodynamic development of a turbine stage has been more and more carried out by using fully 3D Navier-Stokes computations. However the capability of capturing the details of these complex flows (i.e. the wake development or the vortex evolution) and predicting the loss level and distribution with a good accuracy has not been achieved yet. Especially at off-design conditions, where secondary flows are dominant and separated flow regions may be present, the reliability of the results is significantly reduced. The main cause of this failure is the inadequacy of the turbulence models in the computation of these complex flow configurations, even if one or two

Presented at the International Gas Turbine and Aeroengine Congress and Exposition
Cincinnati, Ohio — May 24–27, 1993

equation models are employed.

Referring to recent experimental results (Shizawa and Eaton, 1991, Gregory-Smith and Biesinger, 1992, Perdichizzi et al., 1992), the assumption of isotropic eddy viscosity appears to be inadequate to model complex turbulent flows with intense secondary velocities. Different values have been found for the three eddy viscosities evaluated from the three mean strain and shear stress components. Even negative values of eddy viscosity have been found in significantly extended regions.

The present paper aims to get more insight into the 3D turbulent flow downstream of a turbine cascade at off-design conditions. The effects of incidence angle and pitch to chord ratio on the secondary flow and associated turbulence development have been experimentally investigated. The presented data intend to provide a contribution to clarify the loss production mechanism under off design conditions. These data might be useful in understanding the shortcomings of turbulence models in complex flows and in suggesting modifications for improving their performance.

2. EXPERIMENTAL ARRANGEMENT

The investigation has been carried out on blade cascades scaled from high pressure stage steam turbine nozzles. The blade has an aspect ratio $h/c = 0.91$ and a geometric turning angle $\Delta\beta' = 89.4$ deg; three different pitch-chord ratios $s/c = 0.58, 0.72, 0.87$ have been considered. The cascade geometry and the relevant geometrical data are presented in Fig. 1 and Table 1, whereas the blade profile coordinates have been reported in Perdichizzi and Dossena (1992).

The tests have been performed in the CNPM (Centro Nazionale per Ricerche sulla Propulsione e l'Energetica) transonic wind tunnel for linear cascades. Nevertheless the tunnel is a blowdown type facility, it has been possible to carry out surveys of 3D turbulent flows by hot wire probes, as the tunnel is equipped with a large air storage capacity (3100 kg) allowing for running times of about one hour at low velocity conditions. To prevent from frequent hot wire probe breakdowns, an efficient filtering section with 10 μm pore sintered metal filters has been installed in the settling chamber. A fully automated computer controlled acquisition system, equipped with three stepping motors (one for the azimuthal probe rotation and two for the pitchwise and spanwise traversing), allows a precise probe positioning (with an accuracy of 0.1 mm) and a quite effective data collection. Each step of the probe positioning and of the data acquisition procedure has been carefully optimized to minimize the overall acquisition time. The integration time has been reduced to 250 ms without observing a reduction of the measurement accuracy.

The measurements have been performed in a plane located at $x/b = 1.22$, by traversing both pressure and hot wire probes over a grid of 35 X 13 measuring points. The total pressure and the mean flow velocity components have been measured by using a miniature five hole probe. In each measuring point the turbulence quantities have been evaluated by means of a constant-temperature hot wire anemometer and two single-sensor probes, a first one with a wire normal to the stem and a second with a slanted wire. The system frequency response, deduced from a square-wave test, exceeds 100 kHz. The standard commercial hot wire probes were modified by reducing the prong length, to avoid spurious strain gage effects (Perdichizzi et al., 1989).

For each probe mean and rms voltage readings have been taken at different azimuthal rotations, three for the normal and nine for the slanted probe. The number of the rotations was carefully selected, in order to improve the accuracy of the results and to limit the acquisition time. Through the use of the calibration coefficients related to the King's law and to the Jorgensen's relationship for the angular sensitivity, two overdetermined systems of equations can be written, one for the mean and one for the fluctuating quantities. The solution of these systems by a least square technique provides the mean flow velocities and the six Reynolds stress components in each measuring point. Further details about the experimental apparatus and the measuring technique may be found in Perdichizzi et al. (1989, 1990).

For each test condition the upstream flow has been traversed at

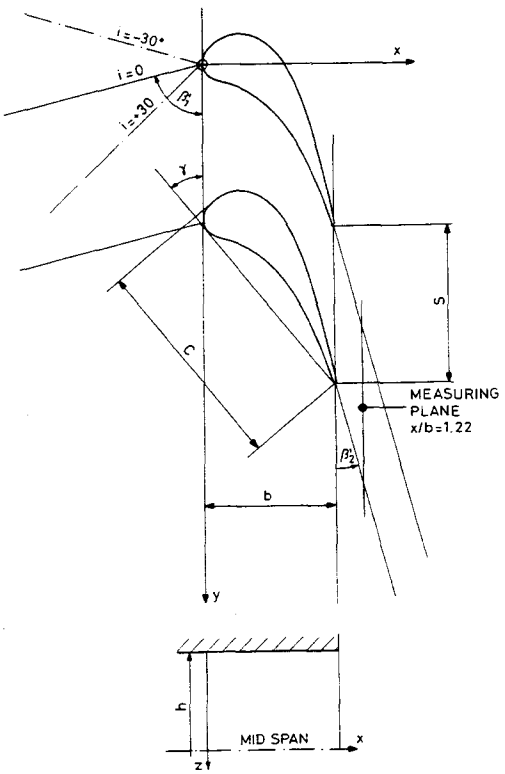

Fig. 1 Cascade geometry.

Table 1 - Cascade geometrical data

Chord length	c	= 55.2 mm
Axial chord	b	= 34.0 mm
Aspect ratio	h/c	= 0.91
Inlet blade angle	β'_1	= 76.1 deg
Outlet blade angle	β'_2	= 14.5 deg
Blade turning angle	$\Delta\beta'$	= 89.4 deg
Stagger angle	γ'	= 39.9 deg

Table 2 - Inlet boundary layer and reference flow conditions

	i = -30	i = 0	i = +30
Displacement thickness, δ^* (mm)	3.37	3.71	3.07
Momentum thickness, θ (mm)	2.31	2.66	2.19
Form factor, H_{12}	1.45	1.39	1.40
Inlet loss, $\zeta_1 \times 100$	1.04	1.45	1.67
Inlet Mach number, M_1	0.071	0.077	0.092
Freestream turbulence, $Tu \times 100$	0.9	0.9	0.9
Outlet Mach number, M_{2is}	0.30	0.30	0.30
Reynolds number, $Re_2 \times 10^6$	0.37	0.37	0.37

Table 3 - Experimental uncertainties

Static and total pressure	± 0.5 %	of the outlet dynamic pressure
Mean velocity from hot wire	± 2 %	
Flow angles from hot wire	± 1.5 deg	
Streamwise and transverse normal Reynolds stress components	± 5 %	
Spanwise normal Reynolds stress component	± 20 %	
Shear Reynolds stress components	± 15 %	

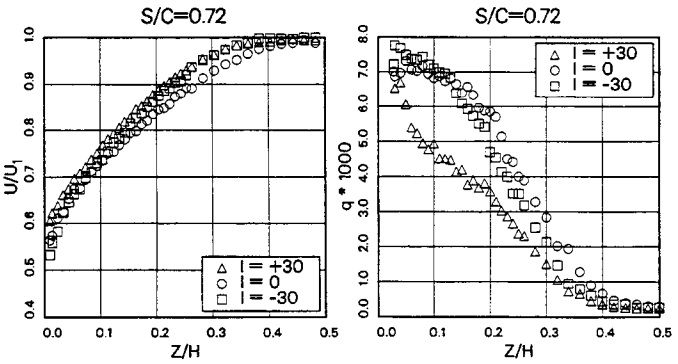

Fig. 2 Inlet boundary layer: mean velocity and turbulence kinetic energy distributions.

x/b = -1.0 by a flattened Pitot tube and by the two hot wire probes, in order to determine the inlet boundary layer characteristics. The mean velocity and the turbulence kinetic energy distributions for the three boundary layers, corresponding to the three incidence conditions, are given in Fig. 2. The inlet boundary layer integral parameters and the reference flow conditions are presented in Table 2.

The experimental uncertainties for pressure probe and hot wire measurements are presented in Table 3. Details about the Reynolds stress error estimation may be found in Perdichizzi et al. (1990).

3. RESULTS AND DISCUSSION

3.1 General considerations and overall results

For each of the three cascades with different pitch-chord ratios, tests have been carried out at three incidence angle i = -30, 0, +30 deg, corresponding to theorical turning angles of 59.4, 89.4 and 119.4 deg. The influence of these parameters on the mean flow field, with particular attention to the secondary flow development, has been already discussed in Perdichizzi and Dossena (1992). It has to be pointed out that the present results refer to a lower expansion ratio, corresponding to an isentropic outlet Mach number M_{2is} = 0.3, against M_{2is} = 0.7 of the previous investigation. For a better comprehension of the presented results, the main mean flow features are briefly summarized.

Referring to the results obtained at the nominal incidence and s/c = 0.87 (see Figs. 4 and 5, middle case), one can clearly observe the typical secondary flow vortex structure. The secondary velocity plots have been obtained by assuming the secondary velocity at a given pitchwise position as the projection of the local velocity vector onto a plane normal to the midspan velocity. There is a well defined passage vortex dominating the flow field and a trailing shed vortex located in the wake region. These two vortices interact on the wake suction side, producing large spanwise velocities towards midspan. A significant crossflow, with the corner vortex embedded in, may be noted in the endwall region. The loss distribution puts in evidence the blade wake, the loss core related to the passage-shed vortex interaction, the endwall loss and the corner vortex loss core.

The turbulence kinetic energy exhibits a distribution similar to the energy loss contours. A relatively low turbulence intensity Tu is present in the wake (about 5 per cent), while higher values (12 per cent) have been found on the suction side of the wake, just where the passage-shed vortex interaction takes place.

The distributions of the normal Reynolds stresses $\overline{u^2}$, $\overline{v^2}$, $\overline{w^2}$, presented in Fig. 5, show that the turbulence is not isotropic.

The $\overline{u^2}$ distribution resembles the one of the energy loss, showing traces of the blade wake and of the low energy cores associated with the passage and corner vortices. A contribution to this component is certainly given by the action of the $\overline{uv}$ and $\overline{uw}$ shear stresses on the mean shear flow; however, the advection operated by the passage vortex is thought to play a significant role in determining this distribution.

The $\overline{v^2}$ component, which results from the dissipation of the transverse mean kinetic energy $V^2/2$, presents a distribution rather similar to the previous component, but the peak values are found to be closer to the shed vortex centre. Significantly higher values for the $\overline{v^2}$ component take place all over the endwall region, extending towards the midspan. This is likely not only due to the dissipation of the secondary kinetic energy of the cross-passage flow, but a significant contribution comes also from the transverse turbulence existing in the inlet boundary layer. A similar feature does not appear in the $\overline{u^2}$ distribution, as the streamwise turbulence of the incoming flow has been reduced by the streamwise flow acceleration (from M_1 = 0.08 to M_2 = 0.30) taking place throughout the cascade.

The distribution of the $\overline{w^2}$ component, which is related to the dissipation of the mean spanwise kinetic energy $W^2/2$, presents a wide core with higher values, if compared to the ones of the other components. This core roughly corresponds to the interaction region of the secondary vortices. In a large region extending from the midspan this component remains small, in accordance with the 2D nature of the flow at midspan.

The $\overline{uv}$ shear stress component, that is the one acting in the blade to blade plane, shows the typical change of sign at the wake centre. This is consistent with the eddy viscosity hypothesis, as opposite transverse gradients of streamwise mean velocity occur through the wake. Higher values are present in the region where the turbulence kinetic energy is high.

The $\overline{uw}$ shear stress component, that is related to the velocity gradients in the through flow plane, shows weakly negative values in the middle of the flow passage with the minimum value on the suction side of the wake at about 30 per cent of the blade span. Positive values are encountered near the endwall. This distribution looks to be in fair agreement with the streamwise velocity gradients along the span $\partial U/\partial z$, as one can derive by observing the loss contour plot.

The $\overline{vw}$ shear stress, that is the component working in the secondary flow plane, shows larger values with respect to the previous components, both for the positive and negative ranges. The high values are principally concentrated in the interaction region between passage and shed vortices. This shear stress is mostly responsible for the secondary kinetic energy decay into turbulent kinetic energy and, therefore, for the secondary loss production downstream of the cascade. The $\overline{vw}$ shear stress distribution appears consistent with the secondary vortex structure. Negative values are associated with the suction side leg of the passage vortex, where positive transverse gradients of the spanwise velocity $\partial W/\partial n$ and large turbulence kinetic energy concentrations are present. Positive values can be noticed in the regions interested by the shed vortex and the corner vortex, both presenting negative transverse

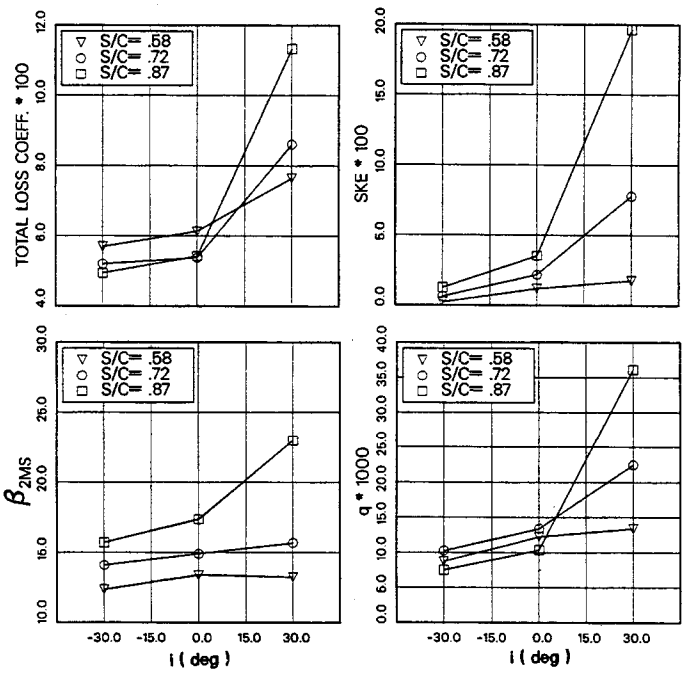

Fig. 3 Mass averaged results versus incidence and pitch to chord ratio.

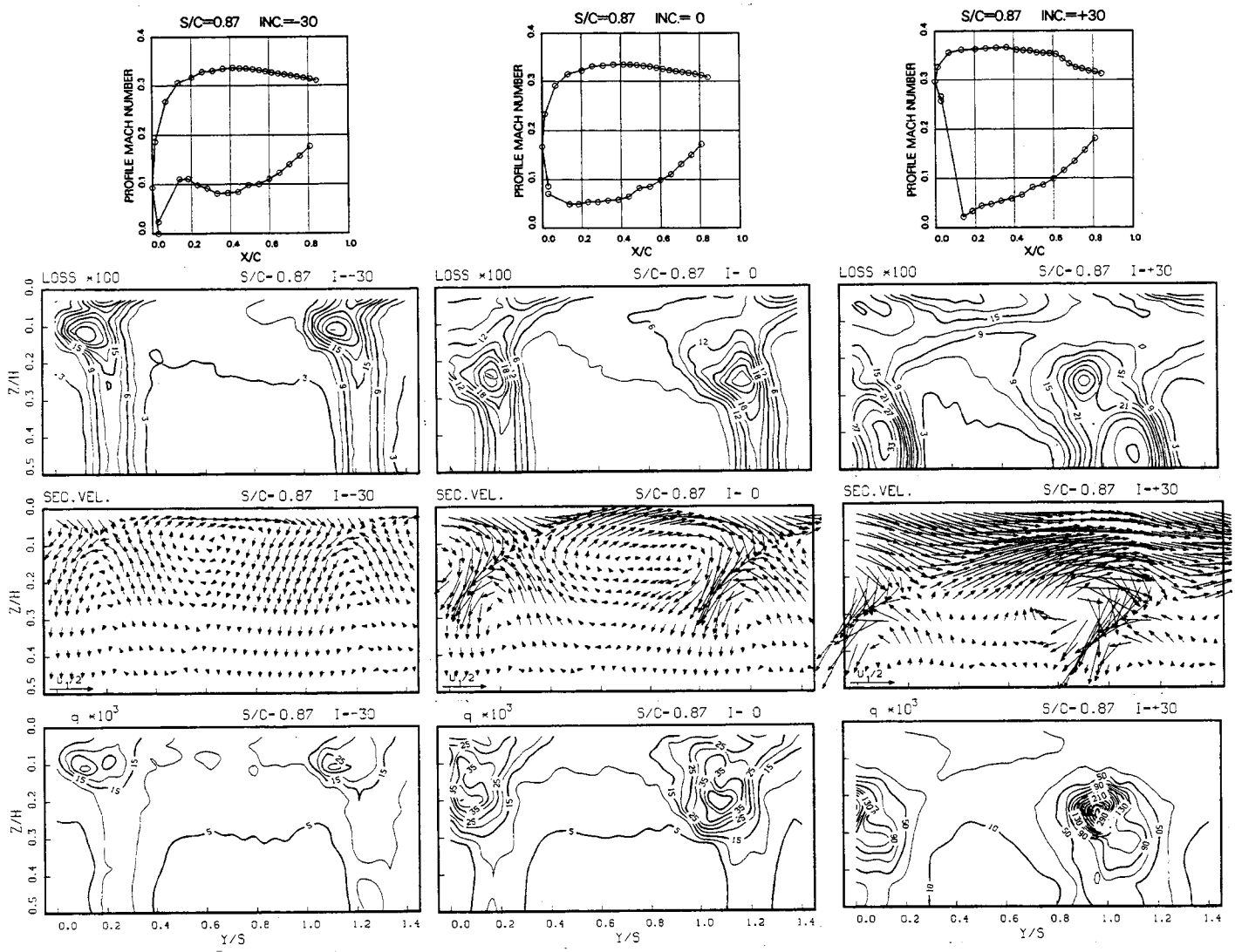

Fig. 4 Profile Mach number distributions, secondary velocity vectors, loss and turbulence kinetic energy contours for s/c = 0.87.

gradients of the mean spanwise velocity.

Similar flow features have been previously observed and described for various cascade geometries by other investigators (e.g. Langston et al., 1977, Marchal and Sieverding, 1977, Gregory-Smith and Graves, 1983, Moore et al., 1987, Gregory-Smith and Cleak, 1990, Perdichizzi et al., 1992).

For each test condition mean and turbulent quantities have been mass averaged over the measuring plane. The overall results for the different pitch-chord ratios versus the incidence angle are displayed in Fig. 3.

Total losses, secondary kinetic energy and turbulence kinetic energy increase with the incidence angle, for all the three pitch-chord ratios. As expected, at the positive incidence the cascade performs well in terms of losses and turbulence intensity when s/c is small, while at s/c = 0.87 a quite uncommon loss level, over 11 per cent, takes place. At negative and nominal incidence angles, better results are obtained when s/c is large.

The pitch-chord ratio exhibits to produce the largest effects at the positive incidence, while the largest variations with the incidence angle occur at the maximum pitch. Thus, these two conditions, i.e. i = +30 and s/c = 0.87, have been selected to analyse in detail the influence of incidence and pitch-chord ratio on the turbulent flow.

3.2 Effects of incidence variation

Mean flow

The results obtained for s/c = 0.87 at i = -30, 0, +30 deg are given in Figs. 4 and 5.

The isentropic Mach number distributions on the blade profile at midspan are given on top of Fig. 4, in order to allow the estimation of the blade loading for the three operating conditions.

The variation of the incidence angle has a direct effect on the flow deflection throughout the cascade, as only limited variations of the outlet flow angle occur (Fig. 3). Consequently significant changes of the blade aerodynamic loading take place, especially on the forward part of the profile which support the larger amount of the flow turning. These changes are responsible for a different blade boundary layer behaviour and, therefore, for the profile loss variation. By increasing the incidence, the stagnation point moves significantly downstream on the pressure side (Fig. 4), producing a larger flow acceleration on the suction side around the leading edge. At i = +30 a higher velocity level is reached on the suction side, but on the rear part of the profile, behind x/c = 0.6, the boundary layer separates, as it can be deduced from the local discontinuity in the Mach number distribution. At i = -30 on the pressure side there is a steep velocity increase followed by an appreciable deceleration extending up to about 30 per cent of the chord. It can't be truly established if a separation bubble exists, as

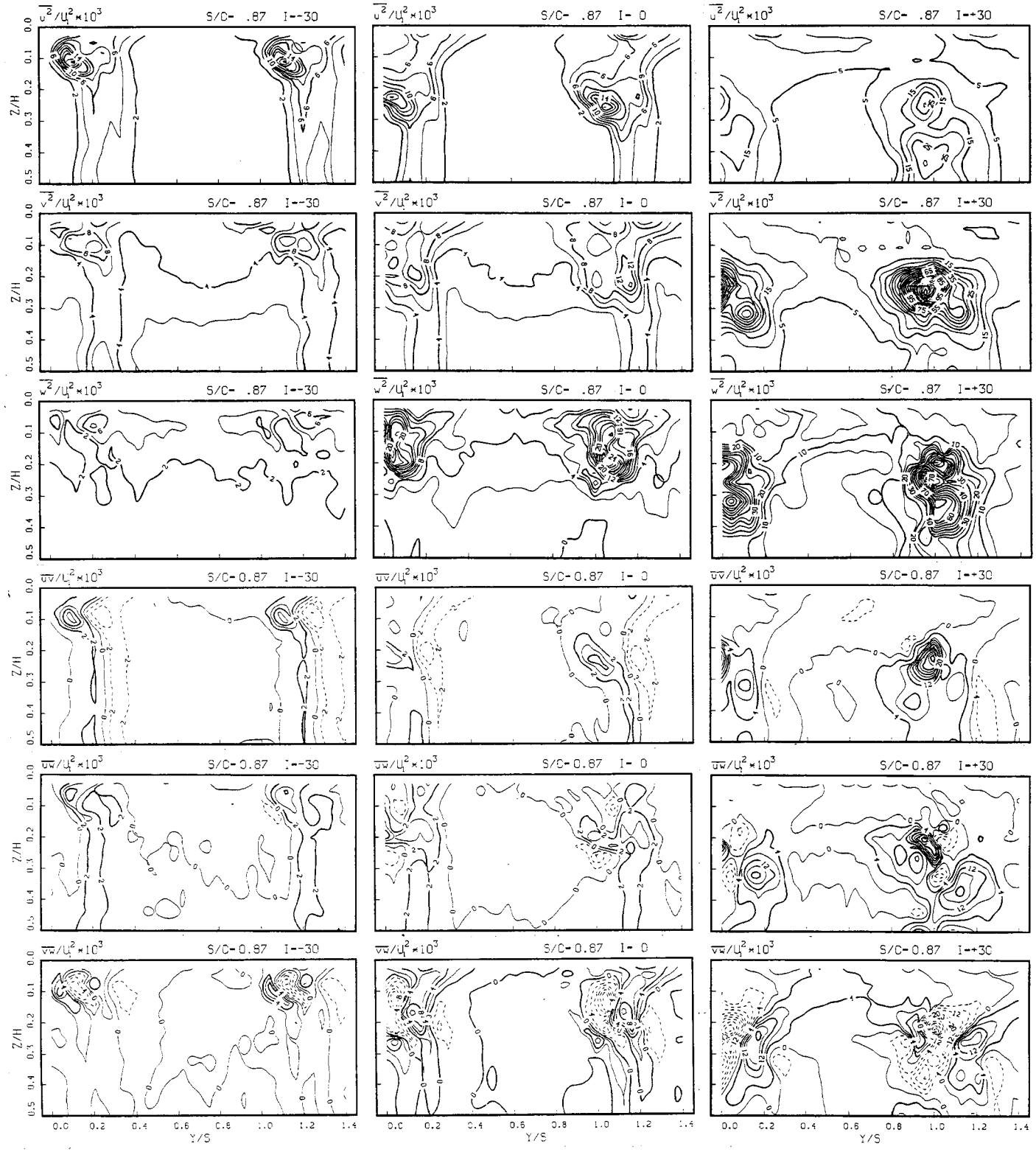

Fig. 5 Reynolds stress components for $s/c = 0.87$.

shown in the results obtained at large negative incidences by Hodson and Dominy (1987), Yamamoto and Nouse (1988) and Perdichizzi and Dossena (1992).

As well known, the incidence variation produces not only the above mentioned 2D effects on the cascade flow, but is also responsible for important variations of the three-dimensional flow field. As a result of the larger blade loading due to incidence angle increase, the secondary flow phenomena undergo a general intensification; indeed larger pressure gradients take place between pressure and suction side just where the passage vortex is developing.

At i = -30 low secondary velocities can be observed all over the flow field. Both passage and shed vortices appear rather weak and confined in the endwall region.

As the incidence increases, the passage vortex strengthens considerably and moves towards the midspan. At i = +30 the secondary velocities become so large as to be comparable to the inlet freestream velocity. It can be noticed that at the endwall there is an impressive crossflow in pitchwise direction, extending up to 20 per cent of the blade height, and that the region interested by secondary flows extends up to reach the midspan. Here the passage and shed vortices of the two half part of the channel come into contact and interact each other.

At i = -30 the loss core associated with the vortex interaction is located on the suction side of the wake near the endwall. As the incidence increases, it widens and moves towards midspan, together with the passage vortex. At i = +30 a second loss core is present in the wake at midspan. This loss region is believed to be produced by the blade boundary layer separation rather than by the trailing shed vortex activity. It is also believed that this separation is not a 2D effect but should be partly promoted by the low energy fluid conveyed to midspan by the passage vortex. Therefore, at this operating condition, because of the strong 3D nature of the flow, midspan losses do not longer represent the profile losses.

Turbulent flow

For all the three incidence conditions, the turbulence kinetic energy contours exhibit a core which follows closely the loss region associated with the passage vortex. This core may be explained by an intense energy production operated by the Reynolds stresses within the passage vortex, as well as by the advection of the turbulent fluid coming from the inlet boundary layer, operated by the passage vortex.

The amount of turbulence kinetic energy appears to be very sensitive to incidence variations. As incidence angle is increased from i = -30 to i = 0 and +30, the peak of the turbulence kinetic energy q varies from 2.5 to 4.5 and 30 per cent of the inlet mean kinetic energy, values which correspond respectively to peaks of turbulence intensity Tu of 9, 12 and 32 per cent of the inlet velocity. This high sensitivity to the flow turning and hence to the blade loading may explain the large differences in the peak values of the turbulence intensity previously found by Moore et al. (1987) (25 per cent), Zunino et al. (1987) (15 per cent), Gregory-Smith and Cleak (1990) (29 per cent) and Perdichizzi et al. (1992) (13 per cent). However, it has to be pointed out that the distributions appear qualitatively similar.

It should be noticed that the peak value of the turbulence kinetic energy at the negative incidence is only about 1 per cent of the corresponding loss peak, while at positive incidence this ratio becomes about 17 per cent. This suggests that, while in the first case the secondary flow field has almost decayed, in the latter case the decay process of the secondary kinetic energy into thermal losses through turbulence is still active. For i = +30 a relatively low turbulence level may be noticed in the wake region, and at midspan there is no evidence of the second turbulent core related to the boundary layer separation on the blade suction surface, previously identified in the loss distribution.

The individual normal stress components (Fig. 5) reflect the effect of the flow turning variation on the secondary flow development.

As incidence is varied, the $\overline{u^2}$ distribution appears to be consistent with the passage vortex behaviour. The core migrates towards the midspan and the peak value undergoes a moderate increase. At i = +30 in the wake region a second core may be observed, which is likely to be connected with the separation previously mentioned.

The $\overline{v^2}$ component shows a dramatic jump from i = 0 to i = +30. This is in agreement with the important increase of the passage vortex intensity and of the related crossflow.

The $\overline{w^2}$ component at i = -30 is weak, as the spanwise velocities are small. At i = 0 the contour lines create an intense core that is consistent with larger spanwise velocities, but at midspan there is not evidence of spanwise turbulence. At i = +30 the core connected with the passage vortex shows a further increase and the hint of a second intensity core appears, possibly associated with the boundary layer separation on the blade suction surface.

For all the examined operating conditions the turbulence is strongly anisotropic. At i = -30 the peak turbulence intensities Tu associated with s, n, z directions are respectively 14, 10 and 8 per cent. At i = 0 the most intense component is the one in the spanwise direction with a peak of 17 per cent, then it follows the streamwise component with 13 per cent and finally the transverse component with 11 per cent. At i = +30 the maximum streamwise turbulence intensity is the 16 per cent, the spanwise component attains the 28 per cent, while the transverse component grows up to 42 per cent.

A similar dependence on the secondary flow configuration may be observed also for the shear stresses. This is an expected feature, as secondary flows operate advection of all mean and turbulence flow quantities; moreover the dissipation of the secondary velocities gives rise to the velocity fluctuations producing both normal and shear stresses.

As incidence increases, the cores of the three components show a clear trend to migrate towards the midspan and a progressive pattern distortion near the endwall, caused by the crossflow strengthening, can be observed.

At i = -30 the absolute value of the $\overline{uv}$ component on the pressure side of the wake is larger than on the suction side. This agrees with a more critical boundary layer development on the pressure side, as in the forward part of the profile the flow experiences an unfavourable velocity gradient caused by the negative incidence (Fig. 4). The core associated with the passage vortex on the suction side of the wake is weak and localized near the endwall. As the incidence increases, it moves from the endwall and, at i = +30, it has strongly grown in comparison with the midspan values associated with the wake.

At i = -30 and i = 0 the $\overline{uw}$ patterns present positive values in the upper part of the loss core and negative in the lower one. In both the regions the $\overline{uw}$ component works against the spanwise gradients of U to make uniform the meridional distribution of the streamwise velocity. At i = +30 there is a much more complicated distribution reflecting the complex flow configuration which has produced three regions with high losses.

The $\overline{vw}$ is the component which undergoes the largest variations for the incidence changes, as it is directly related to the secondary velocities gradients. As the incidence increases, the region interested by significant values widens, in accordance with the larger intensity of the secondary vortices, and the peak values increase several times, from the negative to the positive incidence.

3.3 Effects of pitch-chord ratio variation

The results for the considered pitch-chord ratios at i = +30 are presented in Figs. 6 and 7, respectively for mean and turbulent quantities. Even if the plots for i = +30 and s/c = 0.87 have been already shown in Figs. 4 and 5 for the discussion of the incidence effects, they are here presented again, in order to make easier the analysis of the results versus pitch-chord ratio variation.

Mean Flow

The rise of the pitch-chord ratio produces as a main effect a larger blade loading along the whole profile. Even in this case the final result is the enhancement of the driving force across the blade channel leading to a larger development of secondary flows.

With increasing s/c, the loss coefficient contours show:

- an enlargement of the core associated with the passage vortex and a weak migration towards the midspan;
- a moderate rise of the peak values;
- a general distortion of the contour lines caused by the increasing crossflow.

Only at s/c = 0.87, as previously observed, a second loss core, probably associated with a blade boundary layer separation, stands on the suction side of the wake at midspan.

Turbulence quantities

Turbulence kinetic energy contours follow qualitatively the loss coefficient distribution, but with a relatively larger increase of the peak values.

The cascade pitch-chord ratio produces significant effects on the normal Reynolds stresses, but not as important, as the ones produced by incidence variation.

The $\overline{u^2}$ component distributions reflect the variations of the energy

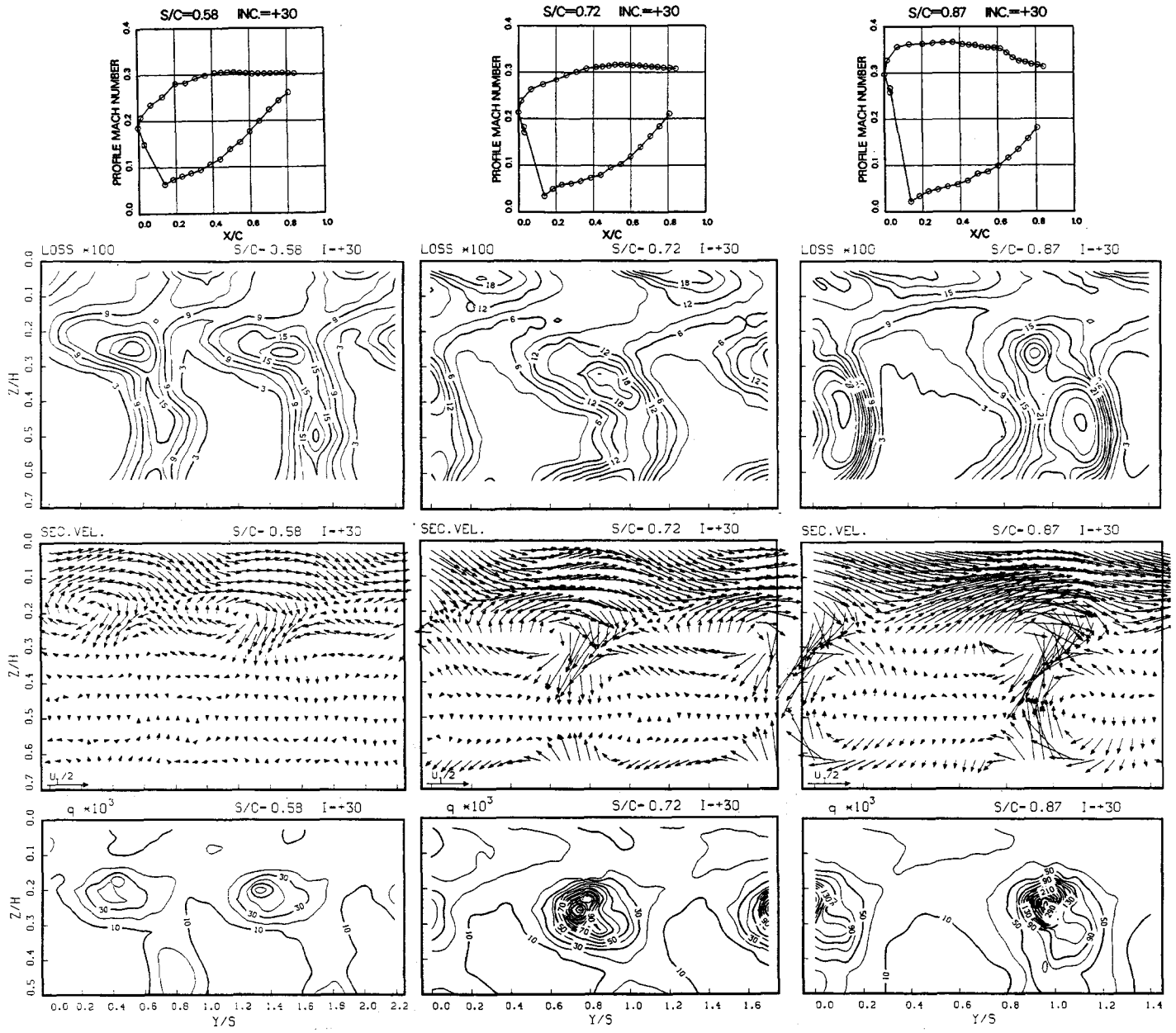

Fig. 6 Profile Mach number distributions, secondary velocity vectors, loss and turbulence kinetic energy contours for i = +30 deg.

loss contours. The turbulence intensity peaks associated with this stress component vary from 10 to 16 per cent, as s/c increases from 0.58 to 0.87.

The $\overline{v^2}$ distribution related to the dissipation of the mean kinetic energy associated with the large crossflow velocities show higher peaks, if compared to the other components, for all the s/c ratios. The turbulence intensity peak associated with this component increases from 16 up to 42 per cent.

The $\overline{w^2}$ component is mainly concentrated in the region of interaction between passage and shed vortex, rather than in the wake. Plots show a peak of relative turbulence varying from 13 to 28 per cent, as the pitch-chord ratio increases.

Pitch-chord ratio variation acts in order to influence the magnitude of the shear stress components rather than to modify substantially their patterns. A common feature of all the distributions is the distortion in the transverse direction of the contour lines in the endwall region. This is related to the convective effect associated with the intense crossflow operating at the present incidence angle.

Referring to the $\overline{uv}$ component, it may be noted that the passage is shared in regions of positive and negative values. The first one, including the suction side of the wake, the passage vortex core and the corner vortex area, widens and becomes more intense as s/c increases.

As expected, the $\overline{uw}$ component becomes more intense at larger pitch-chord ratios. Larger changes occur from s/c = 0.72 to s/c = 0.87, where a second nucleus of $\overline{uw}$ appears, according with a more complex spanwise distribution of the loss coefficient.

Finally the $\overline{vw}$ component shows to be the strongest shear stress and the most sensitive to the secondary flow enhancement.

3.4 Turbulence production

The turbulence production, which is the rate at which mean kinetic energy is converted into turbulence kinetic energy, is the principal mechanism for the generation of total pressure losses. This term can be calculated from experimental data, as the work of deformation of the mean motion operated by the Reynolds stresses $P = -\Sigma_{ij}\overline{u_i u_j}\,U_{i,j}$.

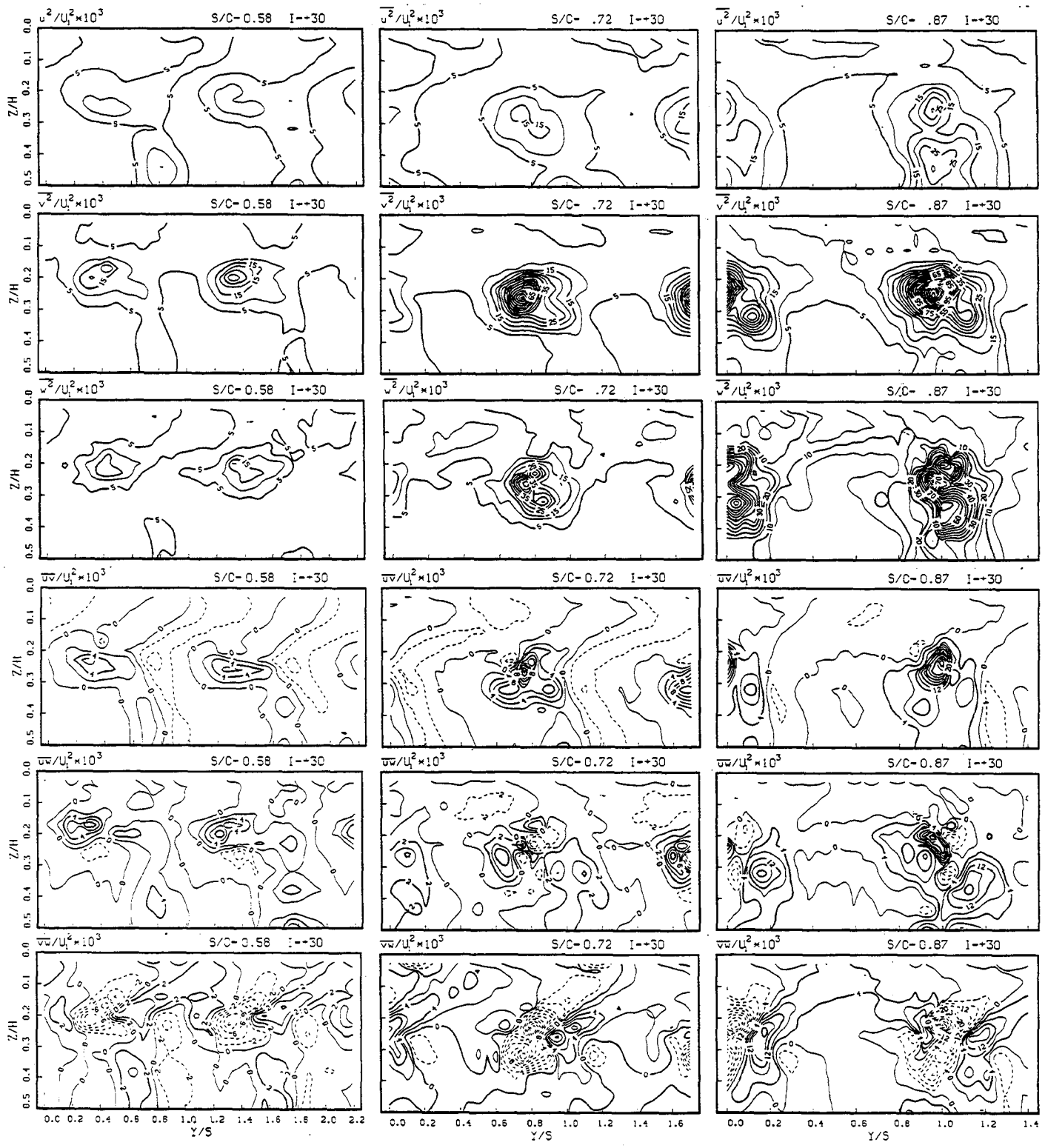

Fig. 7 Reynolds stress components for i = +30 deg.

Moore et al. (1987) were able to calculate the deformation work in the flow field downstream of a turbine cascade, clarifying the mechanisms of loss production and secondary flow decay. They shown that by far the larger contribution to the dissipation of the mean kinetic energy was given by the work of the $\overline{vw}$ stress component in the secondary flow plane. They also found the presence of flow regions where the turbulence production was negative, i.e. energy was returned from turbulence to mean flow.

Further measurements in turbine cascades by Gregory-Smith et al. (1990), Perdichizzi et al. (1992) and in three-dimensional boundary layers by Shizawa and Eaton (1991) confirmed substantially those results.

Fig. 8 shows the effects of flow incidence and cascade pitch-chord

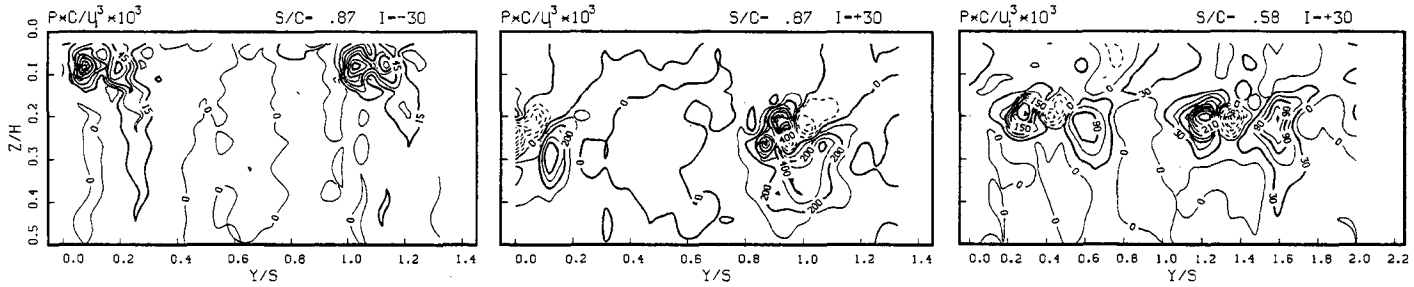

Fig. 8 Turbulence kinetic energy production contours.

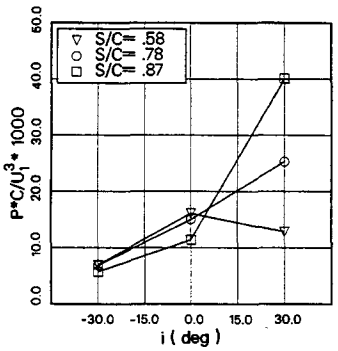

Fig. 9 Area averaged turbulence kinetic energy production versus incidence and pitch to chord ratio.

ratio on the turbulence production distribution for the limiting cases i = -30 s/c = 0.87, i = +30 s/c = 0.87 and i = +30 s/c = 0.58.

To calculate the deformation work, all the nine derivatives of the velocity components had to be computed. The derivatives of the mean velocity component in spanwise and pitchwise directions have been evaluated from the experimental data on the measuring plane, while the ones in the axial direction have been calculated by the continuity equation and by the Crocco relationship, with the assumption of constant total enthalpy (Gregory-Smith et al., 1987; Perdichizzi, 1990). The deformation work has been made non dimensional multiplying it by the factor c / U_1^3.

In all the three cases, the plots show intense cores, consistent with those of the turbulent kinetic energy. Even at i = -30, where the secondary flows are weak, much larger production is associated with the vortex decay rather than with the wake decay. At this incidence, more turbulence production is noticeable on the pressure side of the wake, rather than on its suction side. This is in accordance with the profile Mach number distributions. From i = -30 to i = +30 the cores move from endwall towards the midspan and their peak values grow about ten times. This is the same increasing rate found for the turbulent kinetic energy peak value.

At i = +30 there are two distinct nuclei corresponding respectively to the passage and shed vortex dissipation. For both the pitch-chord ratios a significant region with negative production, located between the two positive cores, may be observed.

For each operating condition the turbulence production has been area averaged over the cascade passage and the results are displayed versus incidence and pitch-chord ratio in Fig. 9.

It can be observed a trend which is similar to the ones shown by turbulence and secondary kinetic energies in Fig. 3. This indicates the strict relationship existing between the turbulence production and the secondary flow intensity. For the smaller pitch-chord ratio the turbulence production is almost insensitive to incidence changes, while for larger s/c great variations take place.

The overall turbulence production results by the sum of nine different terms $P_{ij} = -\overline{u_i u_j}\, U_{i,j}$, which may be grouped three by three to obtain the productions of the individual normal stress components $P_i = -\Sigma_j \overline{u_i u_j}\, U_{i,j}$. These terms provide the rate at which the streamwise, transverse and spanwise components of the mean kinetic energy are converted into the corresponding normal Reynolds stresses.

The area averaged values of the production terms P_i, made non dimensional with respect to the overall turbulence production P, are given in Fig. 10. This plot allows to estimate the relative contribution of each term to the overall turbulence production in the measuring plane for each operating condition.

It may be noticed that for low incidence conditions the greatest part of the turbulence production, i.e. up to 90 per cent, is in the streamwise direction. This means that in the measuring plane the wake mixing process is still active and that the related loss production is dominating with respect to the other loss sources. As the pitch-chord ratio and the incidence angle increase, the importance of this contribution reduces, while transverse and spanwise contributions rise. This may be simply explained by considering that under such conditions the spanwise extent of the pure two-dimensional flow, and hence of the wake, is reducing significantly, while the three-dimensional flow phenomena are acquiring more and more importance. At positive incidence and large pitch-chord ratio the turbulence production in the transverse and spanwise directions accounts respectively for about 40 and 50 per cent of the total.

To complete the set of turbulence data, the mass averaged values of the relative amount of turbulence kinetic energy along the three

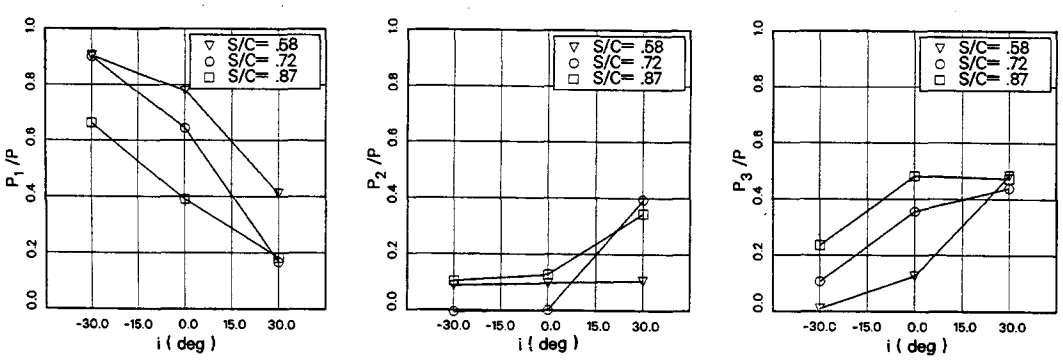

Fig. 10 Area averaged normal Reynolds stress productions versus incidence and pitch to chord ratio.

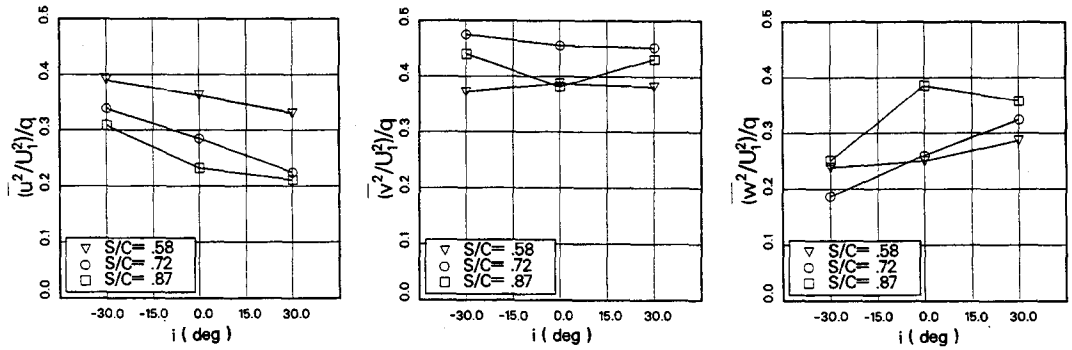

Fig. 11 Mass averaged normal Reynolds stress components versus incidence and pitch to chord ratio.

directions are given in Fig. 11. These data are the result of the dynamic process of production, transport and dissipation of the turbulence occurred from the cascade inlet up to the measuring plane.

The contribution of the streamwise component to the overall kinetic energy presents a decreasing trend with the incidence rise for all the pitch to chord ratios. Higher values, ranging from 38 to 33 per cent, have been found for the smaller pitch-chord ratio. This trend, which is similar to the one of the correspondent production term P_1, even if rather different rates, confirms that the turbulence in the primary direction is mostly due to the wake mixing process.

Conversely, the spanwise component gets up from about 20-25 per cent up to 30-38, as the incidence angle is increased, consequently to the major importance of the secondary flows.

As far as it concerns the transverse turbulence component, it has to be noticed that it remains roughly constant for all the inlet angle conditions, but presenting higher levels with respect to the other components (i.e. at about 40-45 per cent, depending on the pitch-chord ratio). This insensibility to the test conditions and the higher level found even at low incidence is not straightforward. In fact, in a two-dimensional wake, relatively small values of $(\overline{v^2}/U_1^2)/q$ are expected. The distribution of $\overline{v^2}$ for i = -30 and s/c = 0.87 (Fig. 5) suggests that the larger values should be due to the transverse turbulence

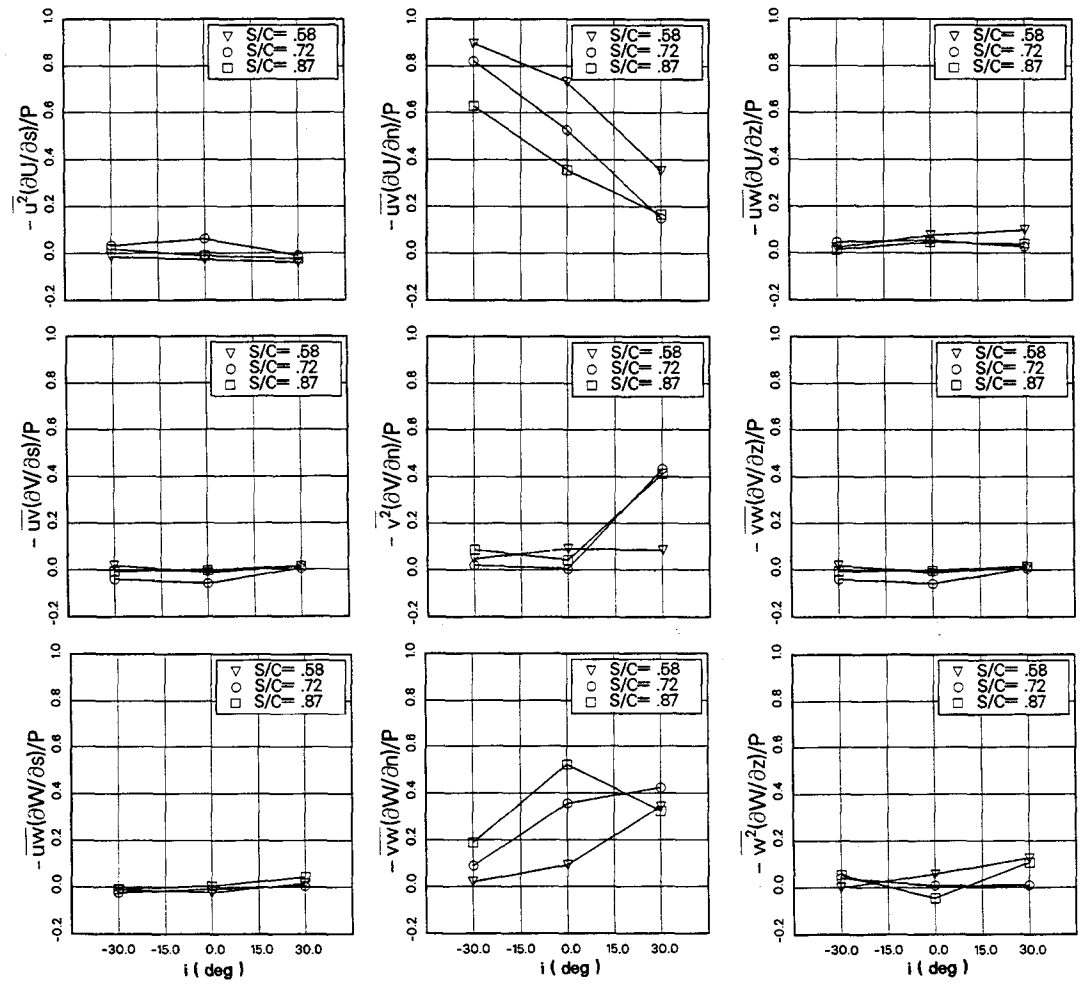

Fig. 12 Area averaged individual contributions to the turbulence production.

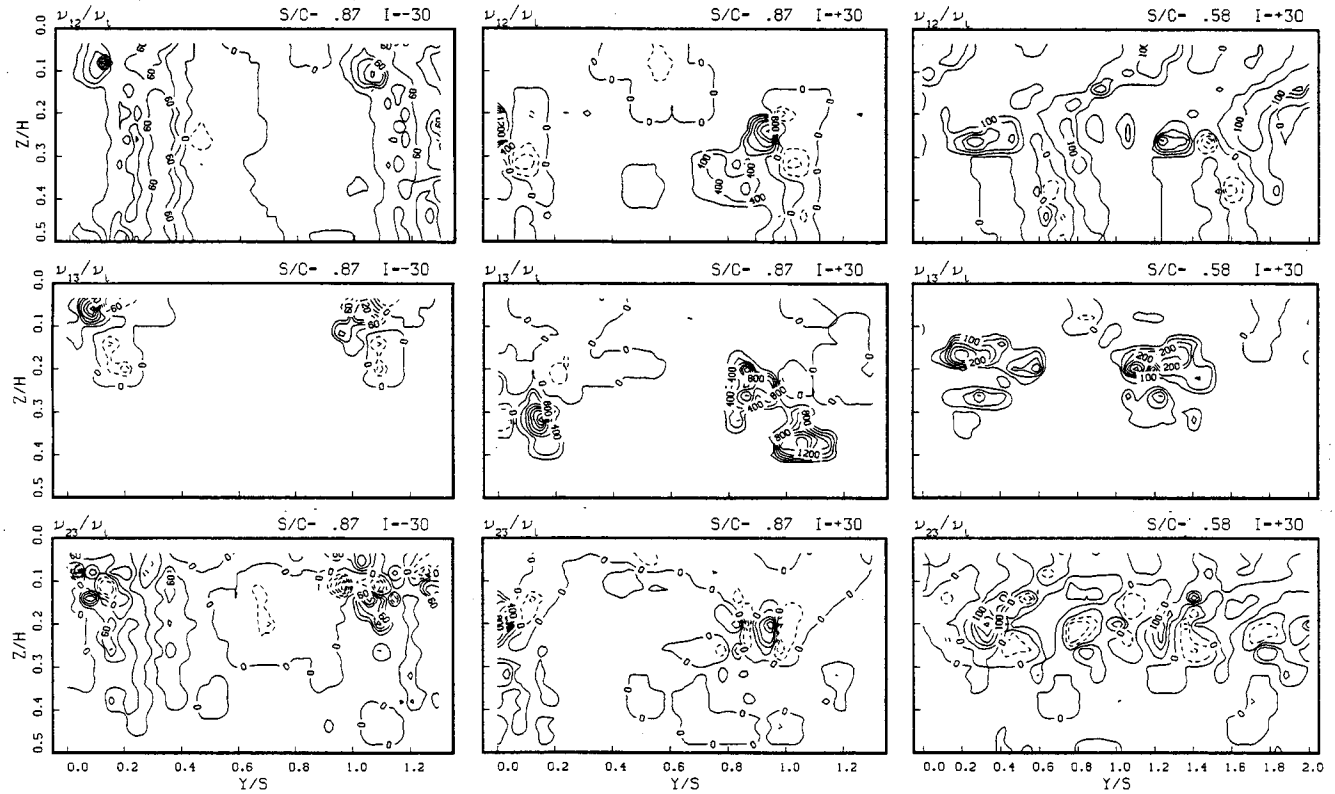

Fig. 13 Eddy viscosities contours.

of the inlet endwall boundary layer conveyed downstream.

The nine terms contributing to overall turbulence production P_{ij}, made non dimensional with respect to P, are given in Fig. 12.

It may be noticed that all the contributions associated with the streamwise deformation of the mean flow $P_{i1} = -\overline{u_i u}\ \partial U_i/\partial s$ remain low for all the test conditions. Especially at negative and zero incidence, they show the trend to produce mean kinetic energy, rather than to dissipate it into turbulence energy.

Also the relative contribution of the three terms associated with the spanwise deformation of the mean motion $P_{i3} = -\overline{u_i w}\ \partial U_i/\partial z$ remains small for all the examined operating conditions.

The relevant contribution to the mean kinetic energy dissipation is therefore given by the terms associated with the transverse deformation of the mean motion $P_{i2} = -\overline{u_i v}\ \partial U_i/\partial n$. Depending on which mean velocity components U, V or W they are based, they contribute to the correspondent Reynolds stress component production.

It appears that the deformation work $P_{12} = -\overline{uv}\ \partial U/\partial n$ is the principal mechanism of the streamwise Reynolds stress normal component production. It represents the action in the blade to blade plane of the shear stress component $\overline{uv}$ against the transverse non uniformity related to blade wakes or low energy fluid concentrations. It looses its relative importance when, due to larger flow turning, the secondary flows acquire more mean kinetic energy and more and more represent the relevant feature of the flow field. This contribution is by far the largest at negative incidence, especially for small pitch-chord ratios. It is still large at zero incidence and drops to less than 20 per cent for $i = +30$ $s/c = 0.72$ and $s/c = 0.87$. However it has to be pointed out that the relative importance of this term depends strongly also on the aspect ratio of the cascade. Moore et al. (1987) found a contribution of this term to the global deformation work of 11 per cent. The measurements were performed in a plane at 10 per cent of an axial chord downstream of a turbine cascade, characterized by a pitch-chord ratio $s/c = 0.78$, a nominal turning angle of 110 deg, but a low aspect ratio $h/c = 0.81$. Gregory-Smith and Biesinger (1992) evaluated a contribution of 50 per cent to the total deformation work (not accounting for the $\overline{vw}$ contributions that could not be measured) for their turbine cascade with a pitch-chord ratio $s/c = 0.85$, a nominal turning angle of 111.4 deg, but with a rather high aspect ratio $h/c = 1.79$.

Figure 12 (second row) shows that at large positive incidence, i.e. $i = +30$ deg, the relevant mean kinetic energy in the transverse direction is mainly dissipated by the action of the normal stress $\overline{v^2}$, rather than by the shear stresses. The contribution by the $\overline{v^2}\ \partial V/\partial n$ term reaches the 40 per cent of the total work, when intense cores of $\overline{v^2}$ are observed at $i = +30$ $s/c = 0.72$ and 0.87 (Fig. 7). Also in the measurements of Moore et al. (1987), this work of deformation appears as the relevant mechanism of dissipation of the mean transverse kinetic energy. From their results it comes out that this term accounts for the 19 per cent of the total deformation work.

Finally Fig. 12 (third row) confirms that, in presence of important secondary flows, the main mechanism of mean kinetic energy dissipation is the term $\overline{vw}\ \partial W/\partial n$. Indeed, at zero and positive incidences, it accounts for a percentage varying from 30 to 50 per cent of the total deformation work.

Eddy viscosities

The eddy viscosity concept, based on the proportionality between the Reynolds stress tensor and the mean strain tensor, is commonly used to explain the experimental distributions of shear stresses. It also appears to be a useful tool in achieving overall qualitative interpretation of the phenomena. On the other hand, this concept is also very popular in the CFD field, as most simple turbulence models (mixing length, one equation models, two equations models) make use of this hypothesis to predict Reynolds stress distributions.

When the mean velocity field and the three shear stress components are available from the experiments, for each measuring point three eddy viscosities can be directly determined as ratio between the shear stresses and the corresponding strain components: $\nu_{ij} = -\overline{u_i u_j}/S_{ij}$

Eddy viscosity distributions derived from experimental data have been presented by Shizawa and Eaton (1991) for the case of a longitudinal vortex interacting with a turbulent boundary layer, by Gregory-Smith and Cleak (1990) and Perdichizzi and al. (1992) for the 3D flow downstream of turbine cascades.

The distributions of the three eddy viscosities, made non

dimensional with respect to the laminar viscosity, are presented in Fig. 13 for the three limiting cascade operating conditions $i = -30$ $s/c = 0.87$, $i = +30$ $s/c = 0.87$ and $i = +30$ $s/c = 0.58$.

The calculation of eddy viscosity from experimental data poses some problems in the zones where the strain tensor components, which appear at the denominator in the eddy viscosity definition, tend to zero. In the region where both strain and shear stress components are very low, the eddy viscosity values have been forced to zero. When the stress components are significant but the strain, changing sign, passes through zero, the eddy viscosity has to be extrapolated from the neighbouring points.

Even overcoming these problems, the eddy viscosity plots look complicated and significant nuclei of negative values are present in most of the diagrams.

Observing each column of Fig. 13, it comes out that the eddy viscosity can not be considered an invariant scalar coefficient, but rather a vectorial quantity.

For both the cases at small pitch-chord ratio and at negative incidence, the peaks of eddy viscosities present values ranging from 100 to 200 times the laminar viscosity. In case of large positive incidence and large pitch-chord ratio, the peak values grow up to 1000 times the laminar viscosity. As the test conditions are changed, the cores seem to move through the passage following approximately the turbulence kinetic energy distribution, but the exact locations of the peaks depend on the magnitude of each of the two turbulence fluctuations contributing to the individual shear stresses and, hence, to the eddy viscosities. In other words the important anisotropy of the turbulence shown by the distributions of the normal Reynolds stresses (Figs. 5 and 7) is here reflected on the anisotropy of the eddy viscosities.

4. CONCLUSIONS

The results of this experimental investigation have shown in detail the effects of incidence angle and pitch-chord ratio on mean and turbulence characteristics of the flow downstream of turbine cascades.

The changes in aerodynamic blade loading, due to variations both in incidence and pitch-chord ratio, have a significant effect on the magnitude and distribution of energy losses and on the intensity of secondary vortices. The secondary flow activity, which is largely sensitive to the two considered parameters influences the production of turbulence kinetic energy, that is an intermediate step towards the dissipation of mechanical energy into heat losses.

When flow turning and passage driving force increase, the Reynolds stress components, especially those associated with the fluctuating velocities in the secondary flow directions $\overline{v^2}$, $\overline{w^2}$, $\overline{vw}$, show important variations. These variations have a large influence on the individual works of deformation of the Reynolds stresses, responsible for the mean kinetic energy dissipation and turbulence production. As incidence and pitch-chord ratio increase, the total work of deformation undergoes an important rise and the relative influence of each of the nine terms of the overall deformation work is also largely modified. As secondary flows become intense, the deformation work $\overline{uv}\,\partial U/\partial n$, that is the main mechanism of dissipation of the streamwise mean kinetic energy, looses importance and most energy is transferred from the secondary flow to turbulence through the $\overline{v^2}\,\partial V/\partial n$ and $\overline{vw}\,\partial W/\partial n$ mechanisms.

Significant region where the turbulence kinetic energy production term is negative, i.e. where energy is returned from turbulence to mean motion, have been also observed for most of the considered test conditions.

The eddy viscosity concept turned out to be useful for a qualitative explanation of the shear stress distribution, but in the complex 3D flows this simple model, based on a constant proportionality between the Reynolds stress and the mean strain tensor components, is not verified because of the relevant turbulence anisotropy. In fact, rather different distributions of the eddy viscosities for each shear stress component have been found. Distributions and magnitude of the eddy viscosities depend on the two cascade parameters investigated, but in any case significant regions of negative eddy viscosity have been observed.

It seems therefore that to compute accurately the stress distributions in these complex 3D turbomachinery flows, especially at off design conditions, the simple eddy viscosity model is not adequate and the solution of the stress transport equations in the full differential or in the simplified algebraic form is probably required. These models can express the details of the complex turbulence features in 3D flows and, therefore, can also account for the different physical conditions that can influence the flow to be modelled. In order to assess and improve the models, it will become more and more opportune to evaluate the individual terms of the transport equations, like production, dissipation, advection and diffusion, making use of detailed and accurate experimental data on mean and turbulence characteristics of 3D turbomachinery flows.

ACKNOWLEDGEMENTS

The authors wish to express their gratitude to the technical staff of CNPM and to G. Barezzani and V. Pasolini, students in mechanical engineering, for their valuable contributions to the experimental work.

REFERENCES

Gregory-Smith, D. G., and Biesinger, Th., 1992, "Turbulence Evaluation within the Secondary Flow Region of a Turbine Cascade", ASME Paper No. 92-GT-60.

Gregory-Smith, D. G., and Graves, C. P., 1983, "Secondary Flows and Losses in a Turbine Cascade", AGARD CP 351, Paper No.17.

Gregory-Smith, D. G., and Cleak, J. G. E., 1990, "Secondary Flow Measurements in a Turbine Cascade with High Inlet Turbulence", ASME Paper No. 90-GT-20.

Gregory-Smith, D. G., Graves, C. P., and Walsh, J. A., 1987, "Growth of Secondary Losses and Vorticity in an Axial Turbine Cascade", ASME Paper No. 87-GT-114.

Hodson, H. P., and Dominy, R. G., 1987, "The Off-Design Performance of a Low Pressure Turbine Cascade", ASME *Journal of Turbomachinery*, Vol. 109, pp. 201-209.

Langston, L. S., Nice, M. L., and Hooper, R. M., 1977, "Three-Dimensional Flow Within a Turbine Cascade Passage", ASME *Journal of Engineering for Power*, Vol. 99, pp. 21-28.

Marchal, P., and Sieverding, C. H., 1977, "Secondary Flows Within Turbomachinery Bladings", AGARD Conf. on Secondary Flows in Turbomachines, AGARD CP 214, Paper No. 11.

Moore, J., Shaffer, D. M., and Moore, J. G., 1987, "Reynolds Stresses and Dissipation Mechanism Downstream of a Turbine Cascade", ASME *Journal of Turbomachinery*, Vol. 109, pp. 258-267.

Perdichizzi, A., 1990, "Mach Number Effects on Secondary Flow Development Downstream of a Turbine Cascade", ASME *Journal of Turbomachinery*, vol. 112, pp. 643-651.

Perdichizzi, A., Ubaldi, M., and Zunino, P., 1989, "Secondary Flows and Reynolds Stress Distributions Downstream of a Turbine Cascade at Different Expansion Ratios", AGARD *Conference on Secondary Flows in Turbomachines*, Luxembourg, AGARD CP-469, Paper No. 6.

Perdichizzi, A., Ubaldi, M., and Zunino, P., 1990, "A Hot Wire Measuring Technique for Mean Velocity and Reynolds Stress Components in Compressible Flow", *Proceedings, 10th Symposium on Measuring Techniques For Transonic and Supersonic Flows in Cascades and Turbomachines*, V.K.I., Brussel, Paper 8.

Perdichizzi, A., and Dossena, V., 1992, "Incidence Angle and Pitch-Chord Effects on Secondary Flows Downstream of a Turbine Cascade", ASME Paper No. 92-GT-184.

Perdichizzi, A., Ubaldi, M., and Zunino, P., 1992, "Reynolds Stress Distribution Downstream of a Turbine Cascade", *Experimental Thermal and Fluid Science*, n. 5, pp. 338-350.

Shizawa, T., and Eaton, J. K., 1991, "Turbulence Measurements for a Longitudinal Vortex Interacting with a Three-Dimensional Turbulent Boundary Layer", AIAA Paper No. 91-0732.

Yamamoto, A., and Nouse, H., 1988, "Effects of Incidence on Three-Dimensional Flows in a Linear Turbine Cascade", ASME *Journal of Turbomachinery*, Vol. 110, pp. 486-496.

Zunino, P., Ubaldi, M., and Satta, A., 1987, "Measurements of Secondary Flows and Turbulence in a Turbine Cascade Passage", ASME Paper No. 87-GT-132.